Sensors and Actuators B 206 (2015) 577–583

Contents lists available at ScienceDirect

Sensors and Actuators B: Chemical

journal homepage: www.elsevier.com/locate/snb

Highly sensitive acetone gas sensor based on porous $ZnFe_2O_4$ nanospheres

Xin Zhou[a], Jiangyang Liu[a], Chen Wang[a], Peng Sun[a,*], Xiaolong Hu[a], Xiaowei Li[a], Kengo Shimanoe[b], Noboru Yamazoe[b], Geyu Lu[a,*]

[a] State Key Laboratory on Integrated Optoelectronics, College of Electronic Science and Engineering, Jilin University, Changchun 130012, People's Republic of China
[b] Department of Energy and Material Sciences, Faculty of Engineering Sciences, Kyushu University, Kasuga-shi, Fukuoka 816-8580, Japan

ARTICLE INFO

Article history:
Received 19 July 2014
Received in revised form 9 September 2014
Accepted 22 September 2014
Available online 30 September 2014

Keywords:
Solvothermal method
$ZnFe_2O_4$
Porous spheres
Acetone sensor

ABSTRACT

Porous $ZnFe_2O_4$ spherical structures built from nanoparticles were successfully synthesized by annealing the precursor, which was synthesized via a simple template-free solvothermal route with ethanol/ethylene glycol (EG) binary solvents. Various techniques were employed for the characterization of the structure and morphology of as-obtained products. The results revealed that the samples were composed of large amounts of porous $ZnFe_2O_4$ nanospheres with an average diameter around 230 nm, which were constructed by plenty of nano-sized primary particles. Moreover, gas sensor based on the as-prepared samples was fabricated and its sensing performances were investigated. It was revealed that the as-fabricated sensor device exhibited excellent selectivity toward acetone at the operating temperature 200 °C and had a response of about 12–30 ppm acetone, which was about 2.5 times higher than that of sensor based on $ZnFe_2O_4$ nanoparticles. The enhancement in gas sensing properties of porous $ZnFe_2O_4$ nanospheres was attributed to their unique structures.

1. Introduction

Compared with the various traditional analytical systems, gas sensors have been acknowledged as simple and inexpensive tools for detection and quantification of toxic, harmful, flammable, and explosive gases. It is well known that gas sensors are the devices composed of active sensing materials coupled with a signal transducer. Therefore, the selection and development of a potential sensing material play an important role in designing high performance of gas sensors. In the past few decades, the progresses in the field of nanotechnology and materials science have paved the way for preparation of numerous new materials with desired morphologies and physical–chemical properties. In particular, oxide semiconductors have received enormous attention for their promising gas sensing application. Up to now, various oxide semiconductors including α-Fe_2O_3 [1,2], SnO_2 [3,4], In_2O_3 [5,6], WO_3 [7,8], ZnO [9,10], NiO [11], etc., were widely investigated and applied in gas sensors due to their advantages such as small dimensions, low cost, low power consumption, on-line operation, and high compatibility with microelectronic processing. In spite of significant achievement in fabricating gas sensors based on oxide semiconductors, developing new sensor strategies for ever increasing sensitivity, selectivity, and reduction of cost represents one of the major scientific challenges owing to growing concerns about air-quality, environmental monitoring, medical diagnosis, and detection of explosive and toxic gases.

The binary oxide semiconductors have been extensively evaluated for their potential application in gas sensors, since previous researches have shown that the gas sensing properties of oxide semiconductors were closely related with their composition, crystalline size, and surface morphology [12–15]. Therefore, research on the novel sensing materials for further improving the performances of sensors is a hot topic. Spinel ferrites (AFe_2O_4, A = Zn, Ni, Cu, Cd, Co), in which the transition metal cation A^{2+} is incorporated into the lattice of the parent structure of ($Fe^{2+}Fe_2{}^{3+}O_4$) [16], are already widely applied in a variety of fields [17–23], which attributes to their environmental friendliness, low preparation cost and high stability. Among them, $ZnFe_2O_4$ has attracted considerable attention as gas sensing material due to its excellent selectively and/or high sensitivity to a certain gas. Research on the intrinsic relationship between morphology/size and gas sensing property has engendered an urgent need for adjustable synthetic strategies, where the size and morphology of the $ZnFe_2O_4$ can be controlled with designed functionalities. Accordingly, various

* Corresponding authors. Tel.: +86 431 85167808; fax: +86 431 85167808.
E-mail addresses: spmaster2008@163.com (P. Sun), lugy@jlu.edu.cn (G. Lu).

http://dx.doi.org/10.1016/j.snb.2014.09.080
0925-4005/

techniques have been employed to prepare $ZnFe_2O_4$ nanostructures with diverse morphologies [24–27]. Many investigations about gas sensors have suggested that sensing materials with porous structures can increase their gas sensing performances, which derives from their large surface area, low density, and surface permeability [28–30]. For this reason, the design and synthesis of porous $ZnFe_2O_4$ nanostructures through a facile, mild, and low cost method still have importantly scientific and practical significance.

In the present work, we successfully synthesized porous $ZnFe_2O_4$ nanospheres assembling with nanoparticles as primary building blocks via a simple one-step solvothermal reaction and the subsequent heat treatment. Various characterizations were carried out to obtain the crystal structural and morphological information of the as-prepared samples. Furthermore, in order to demonstrate the potential applications, the resulting $ZnFe_2O_4$ porous nanospheres were used to fabricate gas sensor devices, which were then tested for response to a variety of gases. Results revealed that the sensor exhibited excellent selectivity toward acetone at the operating temperature of 200 °C, giving a response of 42.1–100 ppm acetone, which was about 4.5 times higher than that of sensor based on $ZnFe_2O_4$ nanoparticles. Moreover, the sensor could detect acetone down to 1 ppm.

2. Experimental

2.1. Synthesis of $ZnFe_2O_4$ nanospheres

All of the chemical reagents involved in the experiment were analytical grade as purchased from Beijing Chemicals Co. Ltd. of China, and directly used without any further purification. In a typical process, 1 mmol of zinc nitrate hexahydrate ($Zn(NO_3)_2{\cdot}6H_2O$) and 2 mmol of ferric nitrate nonahydrate ($Fe(NO_3)_3{\cdot}9H_2O$) were completely dissolved into a 40 mL ethanol–ethylene glycol (EG) mixed soultion (the volume ratio of ethanol and EG is 1:9) under continuous magnetic stirring. After several minutes of stirring, the homogeneous solution was transformed into a 50 mL Teflon-lined stainless steel autoclave, which was then tightly sealed and maintained at 180 °C for 24 h in an oven. Subsequently, the autoclave was allowed to cool down to the room temperature naturally, and the precipitates were collected by centrifugation and washed several times with deionized water and ethanol alternately, then dried in air at 80 °C for 12 h. Finally, the dried precipitates were annealed at 400 °C for 2 h in air atmosphere with a heating rate of 2 °C/min to obtain porous $ZnFe_2O_4$ nanospheres.

2.2. Characterization

The powder X-ray diffraction (XRD) pattern was recorded with a Rigaku D/Max-2550V X-ray diffractometer using high-intensity Cu-Kα radiation (λ = 1.54178 Å) in the range of 20–70° (2θ) to investigate the crystallographic phase of the as-prepared samples. The morphology of the products was examined by field emission scanning electron microscopy (FESEM, JEOL JSM-7500F, operated at an accelerating voltage of 15 kV). The images of transmission electron microscopy (TEM), high-resolution transmission electron microscopy (HRTEM), and the corresponding selected area electron diffraction (SAED) pattern were obtained on a JEOL JEM-2100 microscope operated at an accelerating voltage of 200 kV. The specific surface area was estimated using the Brunauer–Emmett–Tellller (BET) equation based on the nitrogen adsorption isotherm obtained with a Micromeritics Gemini VII apparatus (Surface Area and Porosity System). The pore size distribution was determined with the Barrett–Joyner–Halenda (BJH) method applied to the desorption branch of adsorption–desorption isotherm. Samples were degassed under vacuum at 120 °C for 4 h prior to the measurements.

2.3. Fabrication and measurement of sensor

The fabrication process of a gas sensor can be described as follows: the as-synthesized porous $ZnFe_2O_4$ nanospheres were mixed with an appropriate amount of the deionized water in order to make a homogeneous paste, subsequently, with the help of a small brush the paste was coated on an alumina tube to form a thick sensing film. The alumina tube is about 4 mm in length, 1.2 mm in external diameter, and 0.8 mm in internal diameter, besides, a pair of Au electrodes were installed at the end of the tube, and each electrode was connected with a pair of Pt wires. After drying in air at room temperature, the device was calcined at 400 °C for 2 h [31,32]. Then, a Ni–Cr alloy coil was inserted to the alumina tube as a heater, allowing us to control the operating temperature of the sensor by tuning the heating current. The gas sensing properties of the samples were evaluated with a RQ-2 gas-sensing characterization system. The measurement was processed by a static process: a given amount of the test gas was injected into a closed chamber by a micro-syringe, and the sensor was put into the chamber for the measurement of the sensitive performances. The required concentration of the test gases was obtained by the static liquid gas distribution method, which was calculated by the following equation [2],

$$C = \frac{22.4 \times \Phi \times \rho \times V_1}{M \times V_2} \times 1000 \quad (1)$$

where C (ppm) is the test gas concentration, Φ is the desired liquid volume, ρ (g/mL) is the density of the liquid, V_1 (μL) is the volume of liquid, V_2 (L) is the volume of the test chamber, and M (g/mol) is the molecular weight of the liquid. For comparison, the other gas sensor based on $ZnFe_2O_4$ nanoparticles was fabricated (see ESI Figs. S1† and S2†). The gas response was defined as the ratio between R_a and R_g, where R_a and R_g are the resistances when the sensor was exposed to air and test gas atmosphere, respectively. The response time and recovery time were defined as the time taken by the sensor to achieve 90% of the total resistance change in the case of adsorption and desorption, respectively.

3. Results and discussion

3.1. Structural and morphological characteristics

The morphologies and microstructures of the as-obtained $ZnFe_2O_4$ samples were analyzed by field emission scanning emission microscopy (FESEM), images of which are shown in Fig. 1. Fig. 1a shows the low-magnification FESEM image of the products, which indicates that the as-prepared samples were consisted of a great deal of uniform and dispersed nanospheres with an average diameter of about 230 nm. The high-magnification FESEM image of a single $ZnFe_2O_4$ nanosphere was presented in Fig. 1b, from which detailed morphological information of the nanospheres could be obtained. It can be seen that large amounts of nanoparticles attached together and assembled into porous structure of the sphere. Transmission electron microscopy (TEM) observations and corresponding selected area electron diffraction (SAED) were carried out to acquire more-detailed structural and crystalline information of the as-prepared samples. The typical TEM image of the $ZnFe_2O_4$ nanospheres is depicted in Fig. 1c, and it is obvious that the size and shape of the products were in good accordance with the FESEM observations. The selected area electron diffraction (SAED) pattern is shown in the inset of Fig. 1c. Obviously, the circular pattern composed of bright arcs demonstrated that the $ZnFe_2O_4$ nanospheres were polycrystalline structures in nature [23,33]. A

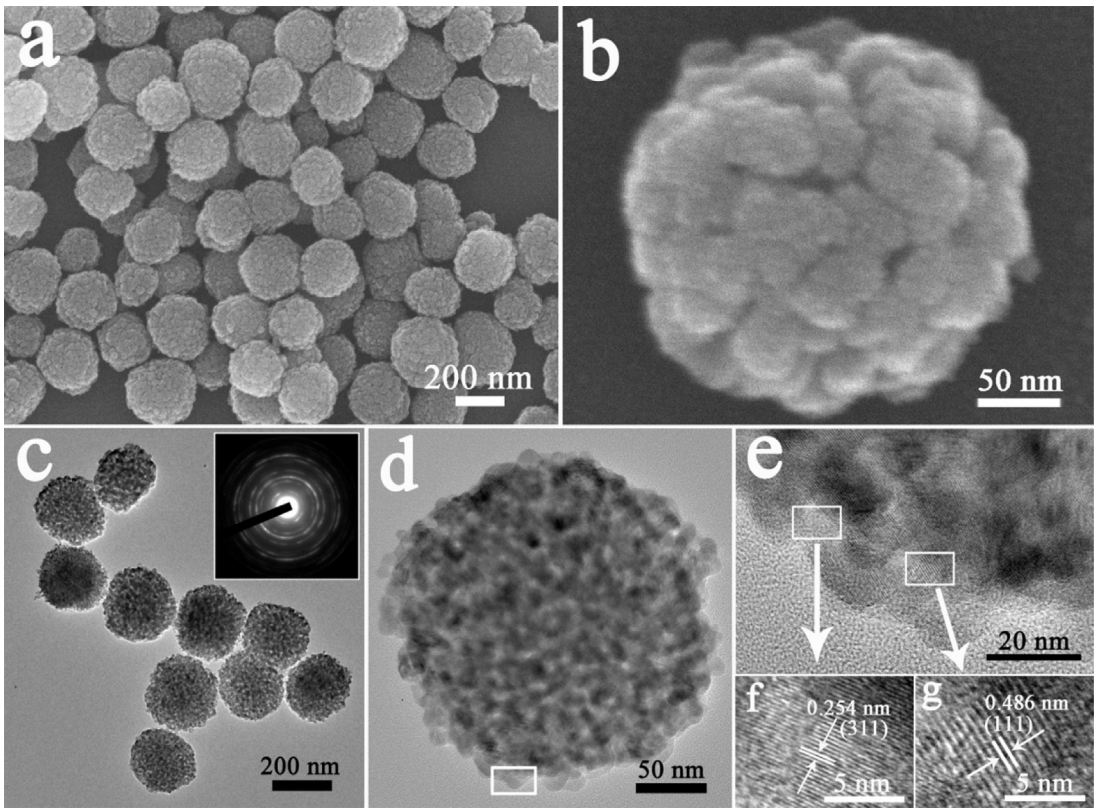

Fig. 1. (a) Low-magnification FESEM image of the porous $ZnFe_2O_4$ spheres. (b) A representative FESEM image of a single $ZnFe_2O_4$ sphere. (c) TEM image of the prepared $ZnFe_2O_4$ samples. (d) TEM image of an individual $ZnFe_2O_4$ sphere. (e) The HRETEM image of the marked section in (d). (f) and (g) are the higher magnifications HRTEM images recorded in different areas of (e). The inset (c) is the corresponding SAED pattern.

representative TEM image of an individual $ZnFe_2O_4$ nanosphere is presented in Fig. 1d, from which it can be clearly seen that a mass of bright spots and nanoparticles existed in the image, indicating that large amounts of nanoscale particles with sizes around several nanometers assembled together formed the porous spherical structure and this further confirmed the FESEM results. Both the porous characteristics and the small crystal size could contribute to the enhancement of gas sensing performances. The high resolution TEM (HRTEM) image (Fig. 1e, which was recorded on the bottom section marked with a white rectangle in Fig. 1d) provided further insight into the structure of the porous spheres. Fig. 1f and g shows the magnified HRTEM images obtained from the marked fringe in Fig. 1e, from which the lattice planes could be clearly observed and the distance between the adjacent planes were measured to be 0.254 nm and 0.486 nm, corresponding to the (3 1 1) and (1 1 1) planes of the cubic $ZnFe_2O_4$.

The powder X-ray diffraction (XRD) pattern of the as-prepared $ZnFe_2O_4$ nanospheres is shown in Fig. 2. All of the recorded diffraction peaks could be well indexed to the pure cubic phase of spinel $ZnFe_2O_4$ with lattice constant of $a = 8.429$ Å, which was in good consistent with those from the standard JCPDS card NO. 89-1010. Furthermore, no diffraction peaks derived from any other impurities could be observed, which indicated the high purity of the sample. It is worth noting that the diffraction peaks were relatively broadened, implying a small crystallite size. The average crystal size of primary $ZnFe_2O_4$ nanoparticles was calculated to be about 8.7 nm by using the Debye–Scherer formula ($D = 0.89\lambda/\beta\cos\theta$, where λ is the X-ray wavelength (1.5418 Å), θ is the Bragg diffraction angle of the peak, and β is the peak width at half maximum) [34]. Compared with the results of FESEM and TEM observations, the calculated value was in good agreement with the FESEM and TEM measurements.

The porosity of sensing material have a great influence for constructing a high performance gas sensor, since the porous structure can enhance the diffusion of the test gas and provide more exposed surface, leading to the high response to test gas. Consequently, the nitrogen adsorption and desorption measurements were carried out to evaluate the porous characteristics of the as-prepared $ZnFe_2O_4$ products. The BET surface area of the porous $ZnFe_2O_4$ spheres was calculated to be 59.0 $m^2\ g^{-1}$. The pore-size distribution of the samples is given in Fig. 3, from which we can clearly see that the $ZnFe_2O_4$ products were formed porous structure with a wide range of pore size distributions from 1 nm to 100 nm, which mainly concentrates in 1–20 nm range. Moreover, the pore volume was measured to be 0.17 $cm^3\ g^{-1}$ from the N_2 adsorption–desorption

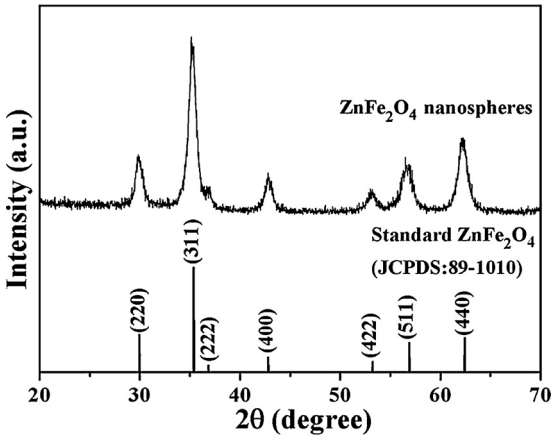

Fig. 2. XRD pattern of the as-obtained $ZnFe_2O_4$ nanospheres.

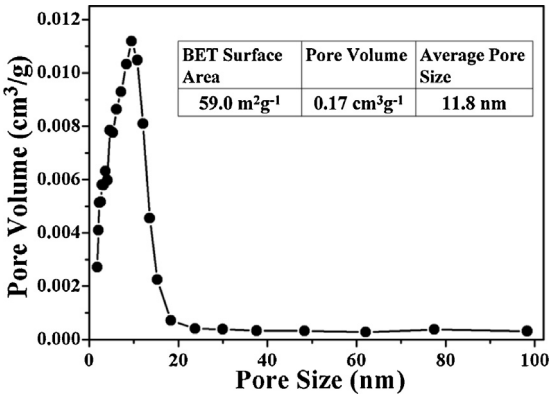

Fig. 3. Pore-size distribution plot of $ZnFe_2O_4$ products.

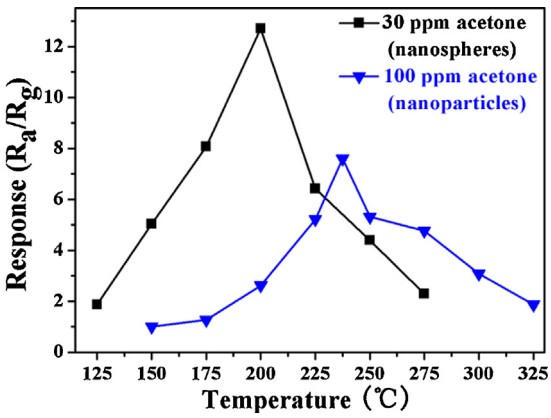

Fig. 4. Response of porous $ZnFe_2O_4$ nanospheres to 30 ppm acetone, response of $ZnFe_2O_4$ nanoparticles to 100 ppm acetone as a function of the operating temperature.

measurement. Such porous structure could provide efficient transport pathways for gas diffusion to the interior of spheres, which would enhance the gas sensing performances of sensor.

3.2. Gas sensing properties

In recent years, environmental pollution and public safety have caused increasing concerns, as a consequent, gas sensors with excellent performances have become a hot topic because they play an important role in gas monitoring. In order to demonstrate the potential application in gas sensing, a gas sensor based on the as-prepared porous $ZnFe_2O_4$ spheres was fabricated and a series of gas sensing measurements were carried out to evaluate its sensing performances. It is well known that the gas response of a gas sensor is highly affected by the operating temperature, hence, the relationships between the operating temperature and gas response of the gas sensor based on porous $ZnFe_2O_4$ spheres and $ZnFe_2O_4$ nanoparticles to 30 ppm and 100 ppm acetone were firstly tested, and the results are shown in Fig. 4. It is clearly to see that the responses to acetone varied with the temperature and both of them exhibited an 'increase–maximum–decrease' tendency. At a low temperature, acetone molecules cannot effectively react with the surface absorbed oxygen species, which led to a low response. While, with the increasing of temperature, both the higher reaction activity and the conversion of surface absorbed oxygen species ($O_{2(gas)} \rightarrow O_{2(ads)} \rightarrow O_2{}^-{}_{(ads)} \rightarrow 2O^-{}_{(ads)}$) contributed to the higher response. After the optimum operating temperature and further increase the temperature, the response reduced because of the low adsorption ability of the acetone molecules, which caused the low utilization rate of the sensing material. Based on the response curve as a function of operating temperature, 200 °C and 237.5 °C were chosen as the optimum operating temperatures for porous $ZnFe_2O_4$ spheres and nanoparticles to go on the further investigations. It is worth noting that the response of the $ZnFe_2O_4$ nanoparticles sensor to 100 ppm acetone was much lower than that of porous $ZnFe_2O_4$ spheres sensor to 30 ppm acetone at 200 °C. The difference in the two sensors can be explained by the $ZnFe_2O_4$ spheres having sufficient porosity that the acetone can easily diffuse throughout nanospheres reaching all available surface reaction sites.

Fig. 5a shows the variation in the responses of sensors using porous $ZnFe_2O_4$ nanospheres and $ZnFe_2O_4$ nanoparticles as a function of the acetone and ethanol concentration at 200 °C. Similar to $ZnFe_2O_4$ nanoparticles, the response of porous nanospheres to acetone and ethanol presented a sharp increase below the concentration of 50 ppm, then, the increasing trend slowed down in the concentration rang of 100–500 ppm, above 500 ppm, the response increased very slowly, indicating that the sensor tended to saturate gradually. When the acetone concentration was low, it can be clearly seen from Fig. 5b that the growth rate of response for porous $ZnFe_2O_4$ nanospheres was much faster than nanoparticles. For $ZnFe_2O_4$ nanoparticles, the response to 5 ppm acetone was almost 1, while for the response of $ZnFe_2O_4$ nanospheres to 800 ppb acetone was about 1.5, which indicated that the sensor based on porous $ZnFe_2O_4$ nanospheres had much lower acetone detection limit than that of sensor based on $ZnFe_2O_4$ nanoparticles. Furthermore, the response of porous $ZnFe_2O_4$ nanospheres to acetone was still much higher than that of the ethanol at the same concentration, which reflected the sensor had excellent selectivity to acetone.

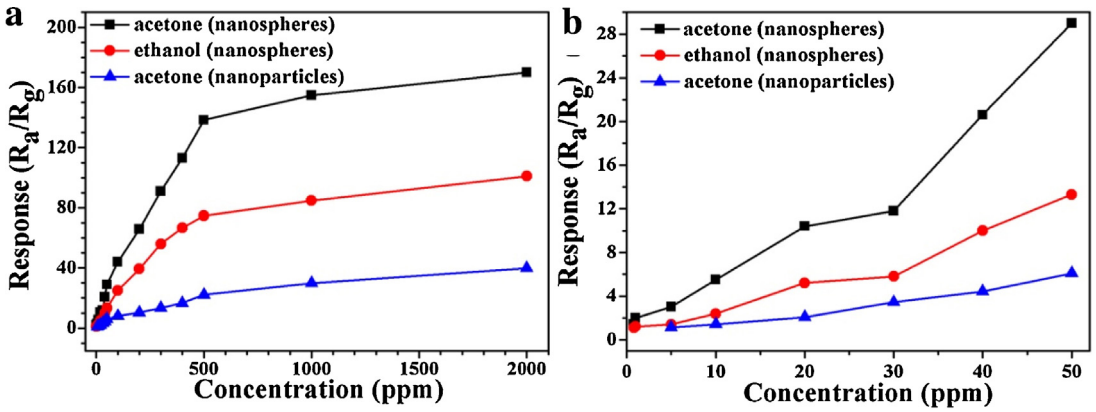

Fig. 5. (a) Response of the sensor using porous $ZnFe_2O_4$ nanospheres versus acetone and ethanol concentrations at 200 °C, and nanoparticles at 237.5 °C. (b) The almost linear concentration dependence of response in the range of 800 ppb–50 ppm for nanospheres and 5–50 ppm for nanoparticles.

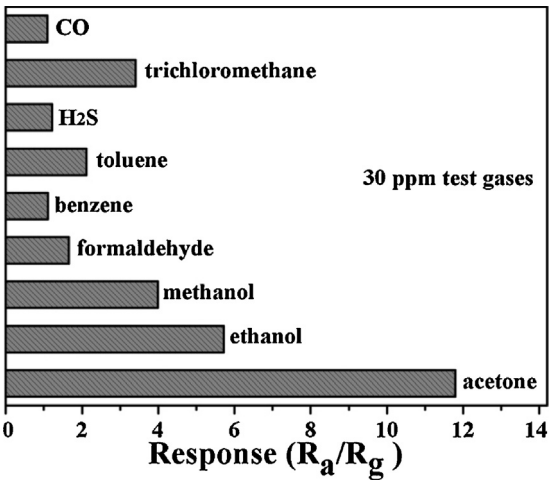

Fig. 6. Response of the sensor based on porous $ZnFe_2O_4$ nanospheres to various test gases with a concentration of 30 ppm at an operating temperature of 200 °C.

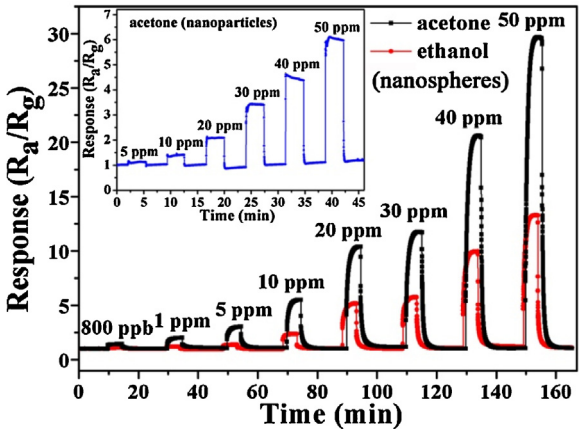

Fig. 8. Dynamic response curves of the gas sensor fabricated by porous $ZnFe_2O_4$ nanospheres to different concentration of acetone and ethanol at 200 °C. The inset is the response transient of $ZnFe_2O_4$ nanoparticles to different concentration of acetone at 237.5 °C.

The selectivity of the as-fabricated porous $ZnFe_2O_4$ nanospheres sensor was evaluated by exposing the sensor to different kinds of gases with a concentration of 30 ppm at 200 °C. Fig. 6 exhibits a bar graph of the responses of the sensor to a variety of gases, such as acetone, ethanol, formaldehyde, methanol, toluene, and so forth. The response toward acetone was remarkably higher than that to the other gases, giving a response of 11.8–30 ppm. Compared with acetone, the sensor exhibited lower response to ethanol, methanol, trichloromethane, and almost no response to CO, H_2S, benzene. Therefore, it is concluded that the as-fabricated gas sensor showed an excellent selectivity toward acetone.

Fig. 7 presents the dynamic response and recovery curves of the sensor using porous $ZnFe_2O_4$ nanospheres to 30 ppm acetone and ethanol at 200 °C. According to the definition of response time and recovery time, the response time to 30 ppm acetone and ethanol at 200 °C were about 9 s and 8 s, respectively, in the same way, the recovery time to 30 ppm acetone and ethanol were about 272 s and 273 s, respectively (shown in Fig. 7b and c). Based on the calculation, the gas sensor showed a relatively rapid response to acetone and ethanol, while the recovery times were a little bit long. Even though, the recovery time are long, the resistance could still return to the initial value in air (R_a). Moreover, the three reversible cycles of the response–recovery curves of the sensor to 30 ppm acetone and ethanol shown in Fig. 7d and e revealed that the gas sensor displayed a stable and repeatable character to both acetone and ethanol.

The response and recovery behaviors were further investigated with the sensor being orderly exposed to different concentration of acetone and ethanol at 200 °C and 237.5 °C for $ZnFe_2O_4$ nanoparticles. It can be seen from Fig. 8 that the characteristics of response and recovery were almost reproducible. Apparently, when the acetone concentration was as low as 800 ppb, the gas response still could reach 1.5, which indicated that the sensor could detect acetone of concentration down to ppb-level. Therefore, this kind of gas sensor with a low detection limit to acetone might be used to monitor acetone which breathed out from the diabetic patient (the average concentration of acetone in the breath from a diabetic patient is believed to be higher than 1.8 ppm) [35]. A comparison between the sensing performances of the sensor fabricated in this work and literature reports for acetone detection is summarized in Table 1. From the table, it can be clearly seen that gas sensor based on the porous $ZnFe_2O_4$ nanospheres exhibited relative higher

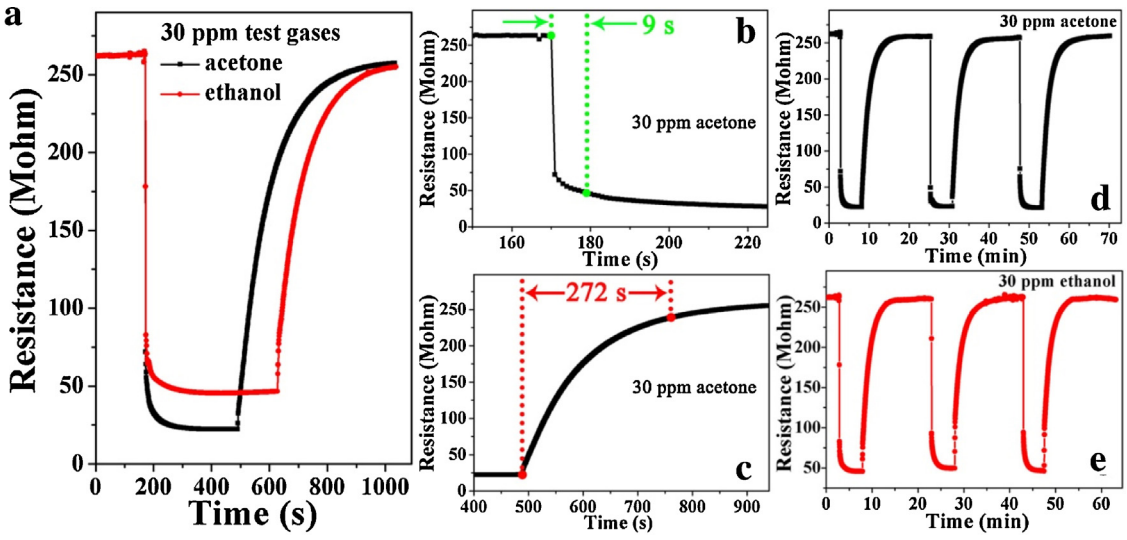

Fig. 7. (a) Response transient of the gas sensor based on porous $ZnFe_2O_4$ nanospheres to 30 ppm acetone and ethanol at 200 °C. (b and c) The dynamic response curve and recovery curve of the porous $ZnFe_2O_4$ nanospheres to 30 ppm acetone. (d and e) Displaying three periods of response–recovery curve to 30 ppm acetone and ethanol, respectively.

Table 1
Comparison of gas-sensing performances of gas sensors based on various $ZnFe_2O_4$ microstructures.

Morphology of $ZnFe_2O_4$	Synthesis approach	Acetone concentration (ppm)	Temperature (°C)	Sensor response	Reference
Nanotubes	Template-engaged sol-gel pyrolysis method	1000	300	18.5	[24]
Nanoparticles	Template-engaged sol-gel pyrolysis method	1000	350	16.8	[24]
Nanoparticles	Sol–gel auto-combustion	500	300	20.1	[26]
Nanoparticles	W/O microemulsion method	50	270	4.2	[36]
Porous nanospheres	Solvothermal method	100	200	42.1	This work

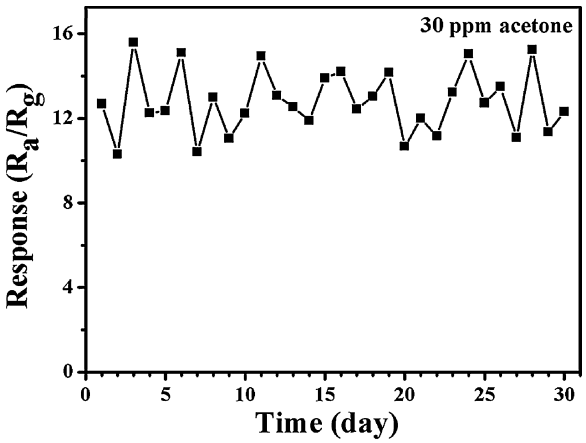

Fig. 9. Long-term stability of the gas sensor based on the as-prepared porous $ZnFe_2O_4$ structures at 200 °C.

acetone response and lower working temperature than those reported in the literatures [24,26,36].

From the view of the practical applications, in order to ensure the accuracy of the detection, gas sensors should maintain good long-term stability. Therefore, the response of the sensor based on porous $ZnFe_2O_4$ nanospheres to 30 ppm acetone was measured, as displayed in Fig. 9. Apparently, even though the response changed every day, the response values were just floating around 12. Hence, a good stability of the porous $ZnFe_2O_4$ nanospheres sensor could be obtained and this favorable gas sensing feature might make the present porous $ZnFe_2O_4$ nanospheres to be particularly attractive as a promising practical sensor.

3.3. Gas sensing mechanism

A popularly and widely accepted sensing mechanism of $ZnFe_2O_4$ sensors is based on the change in resistance of the sensor by the adsorption and desorption process of oxygen molecules on the surface of $ZnFe_2O_4$ [24–26,36]. When the sensor is exposed to air atmosphere, oxygen molecules absorb to the surface of $ZnFe_2O_4$ nanospheres and form $O_2^-{}_{(ads)}$, $O^-{}_{(ads)}$, $O^{2-}{}_{(ads)}$ by capturing free electrons from the conduction band of the sensing material. In this process, oxygen molecules act as electron acceptors, which result in the decrease of electrons concentration and the increase of the resistance of the sensor. On exposure to acetone, ethanol or other reducing gases atmosphere at a moderate temperature, these gas molecules will react with the absorbed oxygen species (Eqs. (2)–(3)). This process releases the trapped electrons back into the conduction band, thereby lowering the measured resistance of sensor.

$$C_3H_6O + 8O^-{}_{(ads)} \rightarrow 3CO_2 + 3H_2O + 8e^- \quad (2)$$

$$C_2H_5OH + 6O^-{}_{(ads)} \rightarrow 2CO_2 + 3H_2O + 6e^- \quad (3)$$

It is well known that both receptor function and transducer function are involved in the working principle of gas sensors based on semiconductors. In addition, the gas response is also determined by the utilization factor of the sensing body [37]. Therefore, the design principles of high performance gas sensor should fully take these three factors into consideration. The good performance of sensor based on porous $ZnFe_2O_4$ nanostructure observed here is likely to be the result of two factors. First, the porous structure promotes the diffusion of gas molecules from outside to the internal and made them efficiently react with the absorbed oxygen species. This means that a high utilization factor of sensing body is obtained, which leads to high response. Second, the crystallite size is small. A mean size of 10 nm is observed (Fig. 1). This causes an important effect: the surfaces of crystallites become significantly more active and likely to absorb oxygen and form ionized oxygen species. Moreover, the size of nanoparticles reaches a scale comparable with the electron depletion layer thickness, which indicates that complete depletion (transducer function) will be achieved. In other words, the high response is obtained [37].

4. Conclusion

In summary, we have developed a simple solvothermal route combined with subsequent heat treatment for the synthesis of porous $ZnFe_2O_4$ nanospheres. FESEM and TEM observations demonstrated that the porous $ZnFe_2O_4$ nanospheres were composed of numerous primary particles with size of around 10 nm. The as-obtained $ZnFe_2O_4$ porous nanospheres were utilized in sensor device and its gas sensing properties were examined. It was found that the device exhibited excellent selectivity toward acetone and was significantly more responsive to this gas than previously reported $ZnFe_2O_4$ sensor devices by giving a response of 11.8–30 ppm acetone, which was about 2.5 times higher than that of $ZnFe_2O_4$ nanoparticles. The enhancement of sensing properties was attributed to the unique porous structure.

Acknowledgements

This work is supported by the National Nature Science Foundation of China (Nos. 61374218, 61134010, and 61327804) and Program for Chang Jiang Scholars and Innovative Research Team in University (No. IRT13018). National High-Tech Research and Development Program of China (863 Program, No. 2013AA030902 and 2014AA06A505).

Appendix A. Supplementary data

Supplementary data associated with this article can be found, in the online version, at http://dx.doi.org/10.1016/j.snb.2014.09.080.

References

[1] X.L. Hu, J.C. Yu, J.M. Gong, Q. Li, G.S. Li, α-Fe_2O_3 nanorings prepared by a microwave-assisted hydrothermal process and their sensing properties, Adv. Mater. 19 (2007) 2324–2329.
[2] P. Sun, W.N. Wang, Y.P. Liu, Y.F. Sun, J. Ma, G.Y. Lu, Hydrothermal synthesis of 3D urchin-like α-Fe_2O_3 nanostructure for gas sensor, Sens. Actuators B: Chem. 173 (2012) 52–57.
[3] E.R. Leite, I.T. Weber, E. Longo, J.A. Varela, A new method to control particle size and particle size distribution of SnO_2 nanoparticles for gas sensor applications, Adv. Mater. 12 (2000) 965–968.

[4] I.S. Hwang, S.J. Kim, J.K. Choi, J.J. Jung, D.J. Dong, K.Y. Dong, B.K. Ju, J.H. Lee, Large-scale fabrication of highly sensitive SnO_2 nanowire network gas sensors by single step vapor phase growth, Sens. Actuators B: Chem. 165 (2012) 97–103.
[5] X.M. Xu, D.W. Wang, J. Liu, P. Sun, Y. Guan, H. Zhang, Y.F. Sun, F.M. Liu, X.S. Liang, Y. Gao, G.Y. Lu, Template-free synthesis of novel In_2O_3 nanostructures and their application to gas sensors, Sens. Actuators B: Chem. 185 (2013) 32–38.
[6] D.H. Zhang, Z.Q. Liu, C. Li, T. Tang, X.L. Liu, S. Han, B. Lei, C.W. Zhou, Detection of NO_2 down to ppb levels using individual and multiple In_2O_3 nanowire devices, Nano Lett. 4 (2004) 1919–1924.
[7] E. Rossinyol, A. Prim, E. Pellicer, J. Arbiol, F.H. Ramirez, F. Peiro, A. Cornet, J.R. Morante, L.A. Solovyov, B.Z. Tian, T. Bo, D.Y. Zhao, Synthesis and characterization of chromium-doped mesoporous tungsten oxide for gas sensing applications, Adv. Funct. Mater. 17 (2007) 1801–1806.
[8] L. You, Y.F. Sun, J. Ma, Y. Guan, J.M. Sun, Y. Du, G.Y. Lu, Highly sensitive NO_2 sensor based on square-like tungsten oxide prepared with hydrothermal treatment, Sens. Actuators B: Chem. 157 (2011) 401–407.
[9] D.W. Wang, S.S. Du, X. Zhou, B. Wang, J. Ma, P. Sun, Y.F. Sun, G.Y. Lu, Template-free synthesis and gas sensing properties of hierarchical hollow ZnO microspheres, CrystEngComm 15 (2013) 7438–7442.
[10] M.L. Yin, S.Z. Liu, Preparation of ZnO hollow spheres with different surface roughness and their enhanced gas sensing property, Sens. Actuators B: Chem. 197 (2014) 58–65.
[11] P. Rai, J.W. Yoon, H.M. Jeong, S.J. Hwang, C.H. Kwak, J.H. Lee, Design of highly sensitive and selective Au@NiO yolk–shell nanoreactors for gas sensor applications, Nanoscale 6 (2014) 8292–8299.
[12] X.F. Chu, D.L. Jiang, Y. Guo, C.M. Zheng, Ethanol gas sensor based on $CoFe_2O_4$ nano-crystallines prepared by hydrothermal method, Sens. Actuators B: Chem. 120 (2006) 177–181.
[13] X.F. Chu, D.L. Jiang, C.M. Zheng, The preparation and gas-sensing properties of $NiFe_2O_4$ nanocubes and nanorods, Sens. Actuators B: Chem. 123 (2007) 793–797.
[14] S. Vijayanand, P.A. Joy, H.S. Potdar, D. Patil, P. Patil, Nanostructured spinel $ZnCo_2O_4$ for the detection of LPG, Sens. Actuators B: Chem. 152 (2011) 121–129.
[15] G.Y. Zhang, B. Guo, J. Chun, MCo_2O_4 (M = Ni, Cu, Zn) nanotubes: template synthesis and application in gas sensors, Sens. Actuators B: Chem. 114 (2006) 402–409.
[16] C.V. Gopal, S.V. Manorama, V.J. Rao, Preparation and characterization of ferrites as gas sensor material, J. Mater. Sci. Lett. 19 (2000) 775–778.
[17] H. Deng, X.L. Li, Q. Peng, X. Wang, J.P. Chen, Y.D. Li, Monodisperse magnetic single-crystal ferrite microspheres, Angew. Chem. Int. Ed. 117 (2005) 2842–2845.
[18] Y.D. Meng, D.R. Chen, X.L. Jiao, Synthesis and characterization of $CoFe_2O_4$ hollow spheres, Eur. J. Inorg. Chem. 2008 (2008) 4019–4023.
[19] U. Luders, A. Barthelemy, M. Bibes, K. Bouzehouane, S. Fusil, E. Jacquet, J.P. Contour, J.F. Bobo, J. Fontcuberta, A. Fert, $NiFe_2O_4$. A versatile spinel material brings new opportunities for spintronics, Adv. Mater. 18 (2006) 1733–1736.
[20] M.Y. Zhu, D.H. Meng, C.J. Wang, G.W. Diao, Facile fabrication of hierarchically porous $CuFe_2O_4$ nanospheres with enhanced capacitance property, ACS Appl. Mater. Interfaces 5 (2013) 6030–6037.
[21] Z.L. Zhang, Y.H. Wang, Q.Q. Tan, Z.Y. Zhong, F.B. Su, Facile solvothermal synthesis of mesoporous manganese ferrite ($MnFe_2O_4$) microspheres as anode materials for lithium-ion batteries, J. Colloid Interface Sci. 398 (2013) 185–192.
[22] C. Cannas, A. Ardu, A. Musinu, D. Peddis, G. Piccaluga, Spherical nanoporous assemblies of iso-oriented cobalt ferrite nanoparticles: synthesis, microstructure, and magnetic properties, Chem. Mater. 20 (2008) 6364–6371.
[23] P.Z. Guo, L.J. Cui, Y.Q. Wang, M. Lv, B.Y. Wang, X.S. Zhao, Facile synthesis of $ZnFe_2O_4$ nanoparticles with tunable magnetic and sensing properties, Langmuir 29 (2013) 8997–9003.
[24] G.Y. Zhang, C.S. Li, F.Y. Cheng, J. Chen, $ZnFe_2O_4$ tubes: synthesis and application to gas sensors with high sensitivity and low-energy consumption, Sens. Actuators B: Chem. 120 (2007) 403–410.
[25] F. Liu, X.F. Chu, Y.P. Dong, W.B. Zhang, W.Q. Sun, L.M. Shen, Acetone gas sensors based on graphene-$ZnFe_2O_4$ composite prepared by solvothermal method, Sens. Actuators B: Chem. 188 (2013) 469–474.
[26] A. Sutka, G. Mezinskis, A. Lusis, D. Jakovlevs, Influence of iron non-stoichiometry on spinel zinc ferrite gas sensing properties, Sens. Actuators B: Chem. 171–172 (2012) 204–209.
[27] M.M. Rahman, S.B. Khan, M. Faisal, A.M. Asiri, K.A. Alamry, Highly sensitive formaldehyde chemical sensor based on hydrothermally prepared spinel $ZnFe_2O_4$ nanorods, Sens. Actuators B: Chem. 171–172 (2012) 932–937.
[28] M. Tiemann, Porous metal oxides as gas sensors, Chem. Eur. J. 13 (2007) 8376–8388.
[29] P. Song, D. Han, H.H. Zhang, J. Li, Z.X. Yang, Q. Wang, Hydrothermal synthesis of porous In_2O_3 nanospheres with superior ethanol sensing properties, Sens. Actuators B: Chem. 196 (2014) 434–439.
[30] X.H. Sun, H.M. Ji, X.L. Li, S. Cai, C.M. Zheng, Open-system nanocasting synthesis of nanoscale α-Fe_2O_3 porous structure with enhanced acetone-sensing properties, Sens. Actuators B: Chem. 600 (2014) 111–117.
[31] X.J. Liu, Z. Chang, L. Luo, X.D. Lei, J.F. Liu, X.M. Sun, Sea urchin-like Ag-α-Fe_2O_3 nanocomposite microspheres: synthesis and gas sensing applications, J. Mater. Chem. 22 (2012) 7232–7238.
[32] P. Sun, L. You, D.W. Wang, Y.F. Sun, J. Ma, G.Y. Lu, Synthesis and gas sensing properties of bundle-like α-Fe_2O_3 nanorods, Sens. Actuators B: Chem. 156 (2011) 368–374.
[33] P.Z. Guo, G.L. Zhang, J.Q. Yu, H.L. Li, X.S. Zhao, Controlled synthesis, magnetic and photocatalytic properties of hollow spheres and colloidal nanocrystal clusters of manganese ferrite, Colloids Surf. A: Physicochem. Eng. Aspects 395 (2012) 168–174.
[34] Z.H. Wei, R.E. Xing, X. Zhang, S. Liu, H.H. Yu, P.C. Li, Facile template-free fabrication of hollow nestlike α-Fe_2O_3 nanostructures for water treatment, ACS Appl. Mater. Interfaces 5 (2013) 598–604.
[35] L. Wang, A. Teleki, S.E. Pratsinis, P.I. Gouma, Ferroelectric WO_3 nanoparticles for acetone selective detection, Chem. Mater. 20 (2008) 4794–4796.
[36] X.S. Niu, W.P. Du, W.M. Du, Preparation and gas sensing properties of ZnM_2O_4 (M = Fe, Co, Cr), Sens. Actuators B: Chem. 99 (2004) 405–409.
[37] N. Yamazoe, G. Sakai, K. Shimanoe, Oxide semiconductor gas sensors, Catal. Surv. Asia 7 (2003) 63–75.

Biographies

Xin Zhou received his BS degree from the Electronics Science and Engineering department, Jilin University, China in 2013. Presently, he is a graduate student and interested in the field of functional materials and gas sensors.

Jiangyang Liu is graduated from Jilin University of China at the Electronics Science and Engineering department in 2014. The same year, she entered the MS course and majored in microelectronics and solid-state electronics.

Chen Wang He is currently working toward the MS degree in the Electronics Science and Engineering department, Jilin University. His research interests include the synthesis of functional materials and their applications in gas sensors.

Peng Sun received his PhD degree from the Electronics Science and Engineering department, Jilin University, China in 2014. Now, he is engaged in the synthesis and characterization of the semiconducting functional materials and gas sensors.

Xiaolong Hu received his BS degree from the Electronics Science and Engineering Department, Jilin University, China in 2011. Presently, he is a PhD student, majored in microelectronics and solid state electronics. Now, he is engaged in the synthesis and characterization of the semiconducting functional materials and gas sensors.

Xiaowei Li received his Master's degree from Electronics Science and Engineering Department, Jilin University, China in 2013. That same year, he entered the PhD course and majored in microelectronics and solid state electronics. Presently, he is engaged in the microwave assisted synthesis and characterization of the semiconducting functional materials and gas sensors.

Kengo Shimanoe has been a professor at Kyushu University since 2005. He received a B. Eng. degree in applied chemistry in 1983 and a M. Eng. degree in 1985 from Kagoshima University and Kyushu University, respectively. He joined Nippon Steel Corp. in 1985, and received a Dr. Eng. degree in 1993 from Kyushu University. His current research interests include the development of gas sensors and other functional devices.

Noboru Yamazoe had been a professor at Kyushu University since 1981 until he retired in 2004. He received his M. Eng. degree in applied chemistry in 1963 and his Dr. Eng. Degree in 1969 from Kyushu University. His research interests were directed mostly to the development and application of functional inorganic materials.

Geyu Lu received the BS degree in electronic sciences in 1985 and the MS degree in 1988 from Jilin University in China and the Dr Eng degree in 1998 from Kyushu University in Japan. Now he is a professor of Jilin University, China. Presently, he is interested in the development of functional materials and chemical sensors.